Propagation of shaped beam through uniaxially anisotropic chiral slab*

Ming-Jun Wang(王明军)[1,4,†], Jia-Lin Zhang(张佳琳)[1], Hua-Yong Zhang(张华永)[2], and Zi-Han Wang(王梓涵)[3]

[1] School of Automation and Information Engineering, Xi'an University of Technology, Xi'an 710048, China
[2] School of Electronics and Information Engineering, Anhui University, Hefei 230039, China
[3] School of Chemistry and Chemical Engineering, Anhui University, Hefei 230039, China
[4] School of Physics and Telecommunications Engineering, Shaanxi University of Technology, Hanzhong 723001, China

(Received 7 March 2020; revised manuscript received 15 June 2020; accepted manuscript online 1 August 2020)

A general solution is obtained to a canonical problem of the reflection and refraction of an arbitrary shaped beam by using a uniaxially anisotropic chiral slab. The reflected, internal as well as refracted shaped beams are expanded in terms of cylindrical vector wave functions, and the expansion coefficients are determined by using the boundary conditions and method of moments procedure. As two typical examples, the normalized field intensity distributions are evaluated for a fundamental Gaussian beam and Hermite–Gaussian beam, and some propagation properties, especially the negative refraction phenomenon, are discussed briefly.

Keywords: shaped beam, uniaxially anisotropic chiral slab, reflection and refraction, negative refraction phenomenon

PACS: 43.20.El, 92.60.Ta **DOI:** 10.1088/1674-1056/abab6c

1. Introduction

Considerable attention has been paid to a chiral medium theoretically and experimentally, due to its unique electromagnetic (EM) properties and wide potential applications. Pendry proposed a chiral design that exhibits many novel properties and provides a new path to achieving the negative refraction.[1] Fedotov *et al*. first investigated the transmission effect of circularly polarized waves through lossy anisotropic planar chiral structures.[2] Tang and Cohen proposed a method to measure the chiral density.[3] Klimov *et al*. designed a two-dimensional lattice of chiral nano-hole in plasma film, whose lattice constant is slightly larger than the wavelength of light, and can be used to control the spatial and polarization characteristics of light beam effectively.[4] Yu *et al*. studied a new class of optical chiral interaction based on complex potentials, and predicted the existence of optical spin black holes.[5] Compared with an isotropic chiral medium, a uniaxially anisotropic chiral (UAC) medium whose chirality appears only in one direction is quite easy to realize artificially, *e.g*., by placing wire spirals or copper springs in the conventional right-handed medium.[6,7] The reflection and refraction of an incident plane wave by such a UAC medium have been investigated by many researchers. Cheng and Cui discussed reflection and refraction properties of plane wave incident from free space into a uniaxial chiral medium.[8,9] Dong and Li investigated the reflection and transmission characteristics of electromagnetic waves through a UAC plate at oblique incidence.[10] However, an incident shaped EM beam rather than a uniform plan wave is often of practical significance and will greatly improve the precision in the modelling of EM beam propagation. For example, the reflection and transmission of an incident Gaussian beam by a uniaxial anisotropic cylinder or slab have been treated by Zhang *et al*.[11] and Wang *et al*.[12] In this paper, we analyze the propagation properties of an arbitrary shaped EM beam through a UAC slab.

We present a theoretical procedure in Section 2 for determining the reflected, internal as well as refracted beams for an shaped beam illuminating a UAC slab. In Section 3, for incidence of a fundamental Gaussian beam and Hermite–Gaussian beam, the normalized field intensity distributions (FIDs) are calculated. Some conclusions are drawn from this work in Section 4.

2. Physical model and formulation

As shown in Fig. 1, an incident shaped beam, described in the Cartesian coordinate system $O'x'y'z'$ (shaped beam coordinate system), propagates from free space to an infinite UAC slab of thickness d. The propagation direction (beam axis $O'z'$) makes an angle β with respect to the axis Oz in the system $Oxyz$. The origin O is on the beam axis and located at

*Project supported by the National Natural Science Foundation of China (Grant No. 61771385), the Science Foundation for Distinguished Young Scholars of Shaanxi Province, China (Grant No. 2020JC-42), the Fund from the Science and Technology on Solid-State Laser Laboratory, China (Grant No. 6142404180301), and the Science and Technology Research Plan of Xi'an City, China (Grant No. GXYD14.26).

†Corresponding author. E-mail: wangmingjun@xaut.edu.cn

© 2020 Chinese Physical Society and IOP Publishing Ltd

$z' = z_0$. The planes $z = 0$ and $z = d$ are the lower and upper surfaces of the UAC slab. In this paper, an $\exp(-\mathrm{i}\omega t)$ time dependence is assumed and suppressed for the EM fields.

To deal with the propagation of an shaped beam through a UAC slab, we adopt a method similar to that described in our previous papers,[11,12] *i.e.*, the EM fields in different regions are expanded in the cylindrical vector wave functions (CVWFs) and the corresponding expansion coefficients will be determined by the boundary conditions.

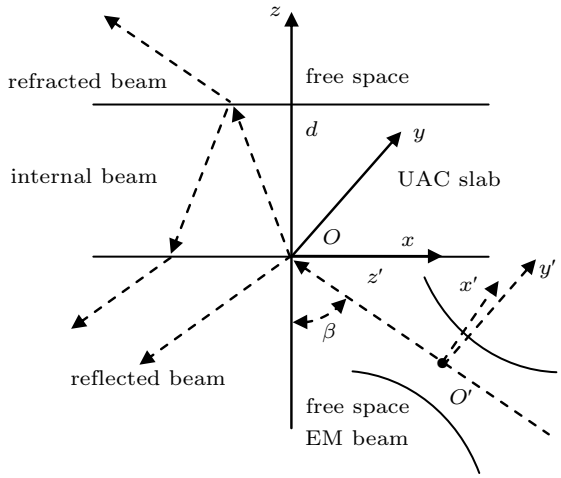


Fig. 1. Infinite UAC slab illuminated by EM beam.

The propagating velocity component along the axis Oz is negative in the half-space $z < 0$ and positive in the half-space $z > d$. Therefore, the reflected wave $(\boldsymbol{E}^{\mathrm{r}}, \boldsymbol{H}^{\mathrm{r}})$ and refracted wave $(\boldsymbol{E}^{\mathrm{t}}, \boldsymbol{H}^{\mathrm{t}})$ can be expressed in terms of the CVWFs as follows:[12,13]

$$\begin{aligned}\boldsymbol{E}^{\mathrm{r}} &= \sum_{m=-\infty}^{\infty}\int_0^{\pi/2}[A_m(\zeta)\boldsymbol{m}_{m\lambda}^{(1)}(-h) \\ &\quad + B_m(\zeta)\boldsymbol{n}_{m\lambda}^{(1)}(-h)]\,\mathrm{e}^{-\mathrm{i}hz}\,\mathrm{d}\zeta, \qquad (1)\\ \boldsymbol{H}^{\mathrm{r}} &= -\mathrm{i}\frac{1}{\eta_0}\sum_{m=-\infty}^{\infty}\int_0^{\pi/2}[A_m(\zeta)\boldsymbol{n}_{m\lambda}^{(1)}(-h) \\ &\quad + B_m(\zeta)\boldsymbol{m}_{m\lambda}^{(1)}(-h)]\,\mathrm{e}^{-\mathrm{i}hz}\,\mathrm{d}\zeta, \qquad (2)\\ \boldsymbol{E}^{\mathrm{t}} &= \sum_{m=-\infty}^{\infty}\int_0^{\pi/2}[C_m(\zeta)\boldsymbol{m}_{m\lambda}^{(1)}(h) \\ &\quad + D_m(\zeta)\boldsymbol{n}_{m\lambda}^{(1)}(h)]\,\mathrm{e}^{\mathrm{i}hz}\,\mathrm{d}\zeta, \qquad (3)\\ \boldsymbol{H}^{\mathrm{t}} &= -\mathrm{i}\frac{1}{\eta_0}\sum_{m=-\infty}^{\infty}\int_0^{\pi/2}[C_m(\zeta)\boldsymbol{n}_{m\lambda}^{(1)}(h) \\ &\quad + D_m(\zeta)\boldsymbol{m}_{m\lambda}^{(1)}(h)]\,\mathrm{e}^{\mathrm{i}hz}\,\mathrm{d}\zeta, \qquad (4)\end{aligned}$$

where $\lambda = k_0\sin\zeta$, $h = k_0\cos\zeta$, while $k_0 = \omega\sqrt{\mu_0\varepsilon_0}$ and $\eta_0 = \sqrt{\mu_0/\varepsilon_0}$ are the free-space wavenumber and characteristic impedance. $A_m(\zeta)$, $B_m(\zeta)$, $C_m(\zeta)$, and $D_m(\zeta)$ are the corresponding expansion coefficients, and the CVWFs $\boldsymbol{m}_{m\lambda}^{(1)}$ and $\boldsymbol{n}_{m\lambda}^{(1)}$ can be found on page 397 in Stratton's book.[13]

Now, we come to consider the constitutive relations for a UAC medium, which are described by[8–10]

$$\boldsymbol{D} = [\varepsilon_t\bar{\bar{I}}_t + \varepsilon_z\hat{z}\hat{z}]\cdot\boldsymbol{E} + \mathrm{i}\kappa\sqrt{\mu_0\varepsilon_0}\hat{z}\hat{z}\cdot\boldsymbol{H}, \qquad (5)$$

$$\boldsymbol{B} = \mu\boldsymbol{H} - \mathrm{i}\kappa\sqrt{\mu_0\varepsilon_0}\hat{z}\hat{z}\cdot\boldsymbol{E}, \qquad (6)$$

where $\bar{\bar{I}}_t = \hat{x}\hat{x} + \hat{y}\hat{y}$, ε_t and ε_z are the transversal and longitudinal permittivity of the UAC medium, and μ and κ are its permeability and chirality parameter respectively

By using the Fourier transform scheme, the EM fields in the UAC medium can be represented as the superposition of eigen plane waves in different directions of propagation as follows:[8–12]

$$\begin{aligned}\boldsymbol{E}^{w} &= \sum_{q=1}^{2}\int k_q^2\sin\theta_k\,\mathrm{d}\theta_k \\ &\quad \times\int_0^{2\pi} f_q(\theta_k,\phi_k)\tilde{\boldsymbol{F}}_q^{\mathrm{e}}(\theta_k,\phi_k)\,\mathrm{e}^{\mathrm{i}\boldsymbol{k}_q\cdot\boldsymbol{r}}\,\mathrm{d}\phi_k, \qquad (7)\\ \boldsymbol{H}^{w} &= -\mathrm{i}\frac{1}{\eta_0}\frac{\mu_0}{\mu}\sum_{q=1}^{2}\int k_q^2\sin\theta_k\,\mathrm{d}\theta_k \\ &\quad \times\int_0^{2\pi} f_q(\theta_k,\phi_k)\tilde{\boldsymbol{F}}_q^{\mathrm{h}}(\theta_k,\phi_k)\,\mathrm{e}^{\mathrm{i}\boldsymbol{k}_q\cdot\boldsymbol{r}}\,\mathrm{d}\phi_k, \qquad (8)\end{aligned}$$

where the wavenumbers k_q ($q = 1, 2$) and EM field eigenvectors $\tilde{\boldsymbol{F}}_q^{\mathrm{e,h}}(\theta_k,\phi_k)$ are given below:

$$k_q = k_t\Big/\sqrt{\frac{1}{A_q}\sin^2\theta_k + \cos^2\theta_k}, \qquad (9)$$

$$A_q = \frac{1}{2}\left(1+\frac{\varepsilon_z}{\varepsilon_t}\right) \pm \sqrt{\frac{1}{4}\left(1-\frac{\varepsilon_z}{\varepsilon_t}\right)^2 + \frac{\mu_0\varepsilon_0\kappa^2}{\varepsilon_t\mu}}, \qquad (10)$$

$$\begin{pmatrix}\tilde{F}_{qx}^{\mathrm{e}} & \tilde{F}_{qy}^{\mathrm{e}} & \tilde{F}_{qz}^{\mathrm{e}}\end{pmatrix} = \begin{pmatrix} -\dfrac{k_{qx}k_{qz}}{k_t^2-k_{qz}^2} - \dfrac{\mathrm{i}k_{qy}k_0\kappa}{k_t^2-k_q^2} & -\dfrac{k_{qy}k_{qz}}{k_t^2-k_{qz}^2} + \dfrac{\mathrm{i}k_{qx}k_0\kappa}{k_t^2-k_q^2} & 1\end{pmatrix}, \qquad (11)$$

$$\begin{pmatrix}\tilde{F}_{qx}^{\mathrm{h}} & \tilde{F}_{qy}^{\mathrm{h}} & \tilde{F}_{qz}^{\mathrm{h}}\end{pmatrix} = \begin{pmatrix} \mathrm{i}\dfrac{k_{qy}}{k_0}\dfrac{k_t^2}{k_t^2-k_{qz}^2} + \dfrac{k_{qz}}{k_0}\dfrac{k_{qx}k_0\kappa}{k_t^2-k_q^2} & -\mathrm{i}\dfrac{k_{qx}}{k_0}\dfrac{k_t^2}{k_t^2-k_{qz}^2} + \dfrac{k_{qz}}{k_0}\dfrac{k_{qy}k_0\kappa}{k_t^2-k_q^2} & -\kappa\dfrac{k_t^2-k_{qz}^2}{k_t^2-k_q^2}\end{pmatrix}, \qquad (12)$$

where $k_t = \omega\sqrt{\varepsilon_t\mu}$, $k_{qz} = k_q\cos\theta_k$, $k_{qx} = k_q\sin\theta_k\cos\phi_k$, and $k_{qy} = k_q\sin\theta_k\sin\phi_k$.

From a physical point of view, the angular spectrum amplitude $f_q(\theta_k,\phi_k)$ in Eqs. (5) and (6) has a period of 2π with respect to ϕ_k, so we can use a Fourier series expansion as

$$f_q(\theta_k,\phi_k) = \sum_{n=-\infty}^{\infty} G'_{nq}(\theta_k)\,\mathrm{e}^{\mathrm{i}n\phi_k}. \qquad (13)$$

The substitution of Eq. (13) into Eq. (7) leads to

$$\boldsymbol{E}^{w} = \sum_{q=1}^{2}\sum_{n=-\infty}^{\infty}\int G'_{nq}(\theta_k)k_q^2\sin\theta_k\,\mathrm{d}\theta_k \times\int_0^{2\pi}\tilde{F}_q^{\mathrm{e}}(\theta_k,\phi_k)\,\mathrm{e}^{\mathrm{i}\boldsymbol{k_q}\cdot\boldsymbol{r}}\,\mathrm{e}^{\mathrm{i}n\phi_k}\,\mathrm{d}\phi_k. \tag{14}$$

Following the same theoretical scheme as that indicated in Refs. [11,12], *i.e.*, substituting the CVWF expansions of arbitrarily polarized EM plane waves $\hat{x}\mathrm{e}^{\mathrm{i}\boldsymbol{k}_q\cdot\boldsymbol{r}}$, $\hat{y}\mathrm{e}^{\mathrm{i}\boldsymbol{k}_q\cdot\boldsymbol{r}}$, and $\hat{z}\mathrm{e}^{\mathrm{i}\boldsymbol{k}_q\cdot\boldsymbol{r}}$ into Eq. (14), where $\boldsymbol{k_q}\cdot\boldsymbol{r} = k_{qx}x + k_{qy}y + k_{qz}z$, we can readily obtain

$$\boldsymbol{E}^{w} = \sum_{q=1}^{2}\sum_{m=-\infty}^{\infty}\int G_{mq}(\theta_k)[\alpha_q^{\mathrm{e}}(\theta_k)\boldsymbol{m}_{m\lambda_q}^{(1)} + \beta_q^{\mathrm{e}}(\theta_k)\boldsymbol{n}_{m\lambda_q}^{(1)} + \gamma_q^{\mathrm{e}}(\theta_k)\boldsymbol{l}_{m\lambda_q}^{(1)}]\exp(\mathrm{i}k_{qz}z)\,\mathrm{d}\theta_k, \tag{15}$$

where

$$G_{mq}(\theta_k) = \frac{2\pi\mathrm{i}^{m-1}}{k_q}G'_{mq}(\theta_k)k_q^2\sin\theta_k,\quad \alpha_q^{\mathrm{e}}(\theta_k) = \frac{-\mathrm{i}k_qk_0\kappa}{k_t^2-k_q^2},$$
$$\beta_q^{\mathrm{e}}(\theta_k) = \mathrm{i}\frac{k_t^2}{k_t^2-k_{qz}^2},\quad \gamma_q^{\mathrm{e}}(\theta_k) = \frac{k_t^2-k_q^2}{k_t^2-k_{qz}^2}\cos\theta_k,$$

and $\lambda_q = k_q\sin\theta_k$.

Due to the phase continuity when using the boundary conditions over the interfaces $z=0$ and $z=d$, we must have $\lambda_q = \lambda$ $(q=1,2)$. Then, from Eq. (15) we can obtain

$$\boldsymbol{E}_1^{w} = \sum_{q=1}^{2}\sum_{m=-\infty}^{\infty}\int_0^{\pi/2}E_{mq}(\zeta)[A_q^{\mathrm{e}}(\zeta)\boldsymbol{m}_{m\lambda}^{(1)} + B_q^{\mathrm{e}}(\zeta)\boldsymbol{n}_{m\lambda}^{(1)} + C_q^{\mathrm{e}}(\zeta)\boldsymbol{l}_{m\lambda}^{(1)}]\exp(\mathrm{i}h_qz)\,\mathrm{d}\zeta, \tag{16}$$

where

$$A_q^{\mathrm{e}}(\zeta) = \frac{-\mathrm{i}k_qk_0\kappa}{k_t^2-k_q^2},\quad B_q^{\mathrm{e}}(\zeta) = \mathrm{i}\frac{k_t^2}{k_t^2-h_q^2},$$
$$C_q^{\mathrm{e}}(\zeta) = \frac{k_t^2-k_q^2}{k_t^2-h_q^2}\frac{h_q}{k_q},\quad k_q = \sqrt{h_q^2+\lambda^2},\quad h_q = \sqrt{k_t^2-\frac{1}{A_q}\lambda^2},$$

and $G_{mq}(\theta_k)\,\mathrm{d}\theta_k = E_{mq}(\zeta)\,\mathrm{d}\zeta$.

Let $\theta_k = \pi - \psi_k$ in Eq. (13) and use the same procedure as that for $\boldsymbol{E}_1^{w}$, then we will obtain

$$\boldsymbol{E}_2^{\mathrm{w}} = \sum_{q=1}^{2}\sum_{m=-\infty}^{\infty}\int_0^{\pi/2}F_{mq}(\zeta)[A_q^{\mathrm{e}}(\zeta)\boldsymbol{m}_{m\lambda}^{(1)}(-h_q) + B_q^{\mathrm{e}}(\zeta)\boldsymbol{n}_{m\lambda}^{(1)}(-h_q) - C_q^{\mathrm{e}}(\zeta)\boldsymbol{l}_{m\lambda}^{(1)}(-h_q)]\exp(-\mathrm{i}h_qz)\,\mathrm{d}\zeta, \tag{17}$$

where $F_{mq}(\zeta)\,\mathrm{d}\zeta = -G_{mq}(\pi-\psi_k)\,\mathrm{d}\psi_k$.

As done in deriving Eqs. (16) and (17) from Eq. (7), the CVWF expansions of the magnetic fields $\boldsymbol{H}_1^{\mathrm{w}}$ and $\boldsymbol{H}_2^{\mathrm{w}}$, corresponding to $\boldsymbol{E}_1^{\mathrm{w}}$ and $\boldsymbol{E}_2^{\mathrm{w}}$, can be conveniently obtained as follows:

$$\boldsymbol{H}_1^{\mathrm{w}} = -\mathrm{i}\frac{1}{\eta_0}\frac{\mu_0}{\mu}\sum_{q=1}^{2}\sum_{m=-\infty}^{\infty}\int_0^{\pi/2}E_{mq}(\zeta)[A_q^{\mathrm{h}}(\zeta)\boldsymbol{m}_{m\lambda}^{(1)} + B_q^{\mathrm{h}}(\zeta)\boldsymbol{n}_{m\lambda}^{(1)} + C_q^{\mathrm{h}}(\zeta)\boldsymbol{l}_{m\lambda}^{(1)}]\,\mathrm{e}^{\mathrm{i}h_qz}\,\mathrm{d}\zeta, \tag{18}$$

$$\boldsymbol{H}_2^{\mathrm{w}} = -\mathrm{i}\frac{1}{\eta_0}\frac{\mu_0}{\mu}\sum_{q=1}^{2}\sum_{m=-\infty}^{\infty}\int_0^{\pi/2}F_{mq}(\zeta)[A_q^{\mathrm{h}}(\zeta)\boldsymbol{m}_{m\lambda}^{(1)}(-h_q) + B_q^{\mathrm{h}}(\zeta)\boldsymbol{n}_{m\lambda}^{(1)}(-h_q) - C_q^{\mathrm{h}}(\zeta)\boldsymbol{l}_{m\lambda}^{(1)}(-h_q)]\exp(-\mathrm{i}h_qz)\,\mathrm{d}\zeta, \tag{19}$$

where

$$A_q^{\mathrm{h}}(\zeta) = \mathrm{i}\frac{k_q}{k_0}\frac{k_t^2}{k_t^2-h_q^2},\quad B_q^{\mathrm{h}}(\zeta) = -\mathrm{i}\kappa\frac{k_t^2}{k_t^2-k_q^2},$$
$$C_q^{\mathrm{h}}(\zeta) = -\kappa\frac{h_q}{k_q}.$$

It should be pointed out that $\boldsymbol{E}_1^{\mathrm{w}}$, $\boldsymbol{H}_1^{\mathrm{w}}$, and $\boldsymbol{E}_2^{\mathrm{w}}$, $\boldsymbol{H}_2^{\mathrm{w}}$ represent the shaped beams within the UAC slab that respectively propagate towards the interfaces $z=d$ and $z=0$.

The unknown expansion coefficients $A_m(\zeta)$, $B_m(\zeta)$, $C_m(\zeta)$, $D_m(\zeta)$ in Eqs. (1)–(4) and $E_{mq}(\zeta)$, $F_{mq}(\zeta)$ $(q=1,2)$ in Eqs. (14)–(19) can be determined by using the boundary conditions at the interfaces $z=0$ and $z=d$, and they are given as follows:

$$\left.\begin{aligned}\hat{z}\times(\boldsymbol{E}^{i}+\boldsymbol{E}^{\mathrm{r}}) &= \hat{z}\times(\boldsymbol{E}_1^{\mathrm{w}}+\boldsymbol{E}_2^{\mathrm{w}})\\ \hat{z}\times(\boldsymbol{H}^{i}+\boldsymbol{H}^{\mathrm{r}}) &= \hat{z}\times(\boldsymbol{H}_1^{\mathrm{w}}+\boldsymbol{H}_2^{\mathrm{w}})\end{aligned}\right\}\quad \text{at } z=0\ , \tag{20}$$

$$\left.\begin{aligned}E_{1r}^{\mathrm{w}}+E_{2r}^{\mathrm{w}} &= E_r^{\mathrm{t}} \quad E_{1\phi}^{\mathrm{w}}+E_{2\phi}^{\mathrm{w}} = E_\phi^{\mathrm{t}}\\ H_{1r}^{\mathrm{w}}+H_{2r}^{\mathrm{w}} &= H_r^{\mathrm{t}} \quad H_{1\phi}^{\mathrm{w}}+H_{2\phi}^{\mathrm{w}} = H_\phi^{\mathrm{t}}\end{aligned}\right\}\quad \text{at } z=d, \tag{21}$$

where $\boldsymbol{E}^{i}$ and $\boldsymbol{H}^{i}$ represent the electric and magnetic fields of the incident shaped beam, and the subscripts r and ϕ respectively denote the r and ϕ components of the EM field.

Now we insert Eqs. (1), (2), and (16)–(19) into Eq. (20), dot-multiply the obtained equations by the CVWFs $\boldsymbol{m}_{(-m')\lambda'}^{(1)}(h')$ and $\boldsymbol{n}_{(-m')\lambda'}^{(1)}(h')$, where $\lambda' = k_0\sin\psi$ and $h' = k_0\cos\psi$, and integrate over the surface $z=0$. After performing the above mathematical operation, we can finally obtain

$$\frac{h}{k_0}B_m(\zeta) + \sum_{q=1}^{2}E_{mq}(\zeta)\left[B_q^{\mathrm{e}}(\zeta)\frac{h_q}{k_q} - \mathrm{i}C_q^{\mathrm{e}}(\zeta)\right] + \sum_{q=1}^{2}F_{mq}(\zeta)\left[-B_q^{\mathrm{e}}(\zeta)\frac{h_q}{k_q} + \mathrm{i}C_q^{\mathrm{e}}(\zeta)\right] = \frac{\mathrm{i}}{2\pi(-1)^m}\frac{h}{\lambda}\int_0^{\infty}r\,\mathrm{d}r\int_0^{2\pi}\boldsymbol{E}^{i}|_{z=0}\times\boldsymbol{m}_{(-m)\lambda}^{(1)}\cdot\hat{z}\,\mathrm{d}\varphi, \tag{22}$$

$$-A_m(\zeta) + \sum_{q=1}^{2}E_{mq}(\zeta)A_q^{\mathrm{e}}(\zeta) + \sum_{q=1}^{2}F_{mq}(\zeta)A_q^{\mathrm{e}}(\zeta) = \frac{1}{2\pi\mathrm{i}(-1)^{m'}}\frac{k_0}{\lambda}\int_0^{\infty}r\,\mathrm{d}r\int_0^{2\pi}\boldsymbol{E}^{i}|_{z=0}\times\boldsymbol{n}_{(-m)\lambda}^{(1)}\cdot\hat{z}\,\mathrm{d}\phi, \tag{23}$$

$$\frac{h}{k_0}A_m(\zeta) + \sum_{q=1}^{2}E_{mq}(\zeta)\left[B_q^{\mathrm{h}}(\zeta)\frac{h_q}{k_q} - \mathrm{i}C_q^{\mathrm{h}}(\zeta)\right] + \sum_{q=1}^{2}F_{mq}(\zeta)\left[-B_q^{\mathrm{h}}(\zeta)\frac{h_q}{k_q} + iC_q^{\mathrm{h}}(\zeta)\right] = \frac{\mathrm{i}}{2\pi(-1)^m}\frac{h}{\lambda}\mathrm{i}\eta_0\int_0^{\infty}r\,\mathrm{d}r\int_0^{2\pi}\boldsymbol{H}^{i}|_{z=0}\times\boldsymbol{m}_{(-m)\lambda}^{(1)}\cdot\hat{z}\,\mathrm{d}\varphi, \tag{24}$$

$$B_m(\zeta)-\sum_{q=1}^{2}E_{mq}(\zeta)A_q^{\rm h}(\zeta)-\sum_{q=1}^{2}F_{mq}(\zeta)A_q^{\rm h}(\zeta)$$
$$=\frac{\mathrm{i}}{2\pi(-1)^{m'}}\frac{k_0}{\lambda}\mathrm{i}\eta_0\int_0^{\infty}r\mathrm{d}r\int_0^{2\pi}\boldsymbol{H}^i|_{z=0}\times\boldsymbol{n}_{(-m)\lambda}^{(1)}\cdot\hat{z}\mathrm{d}\phi. \quad (25)$$

The derivation of Eqs. (21)–(25) is straightforward by using the r, ϕ, and z components of the CVWF, with consideration of the following formulas:[14]

$$\int_0^{2\pi}\mathrm{e}^{\mathrm{i}(m-m')\varphi}\mathrm{d}\varphi=\begin{cases}0, & m\neq m',\\ 2\pi, & m=m',\end{cases} \quad (26)$$

$$\frac{\delta(\lambda-\lambda')}{\lambda}=\int_0^{\infty}\mathrm{J}_n(\lambda r)\mathrm{J}_n(\lambda' r)r\mathrm{d}r, \quad (27)$$

where $\mathrm{J}_n(\cdot)$ denotes the Bessel function of the first kind and $\delta(\lambda-\lambda')$ is the Dirac delta function.

In Eqs. (22)–(25) we have used the vector identity $\boldsymbol{b}\times\boldsymbol{c}\cdot\boldsymbol{a}=\boldsymbol{c}\times\boldsymbol{a}\cdot\boldsymbol{b}$, where $\boldsymbol{a}$, $\boldsymbol{b}$, and $\boldsymbol{c}$ are vector functions, which, for example, will lead to $\hat{z}\times\boldsymbol{E}^i\cdot\boldsymbol{m}_{(-m)\lambda}^{(1)}=\boldsymbol{E}^i\times\boldsymbol{m}_{(-m)\lambda}^{(1)}\cdot\hat{z}$.

It can be explained that the method of moments (MoM) procedure is used to obtain Eqs. (22)–(25), by choosing appropriate CVWFs as basis functions and weighting functions.

By inspecting the EM fields expansions in Eqs. (3), (4), and (16)–(19) into Eq. (21), we can have the following equations:

$$\sum_{q=1}^{2}E_{mq}(\zeta)A_q^{\rm e}(\zeta)\mathrm{e}^{\mathrm{i}h_qd}+\sum_{q=1}^{2}F_{mq}(\zeta)A_q^{\rm e}(\zeta)\mathrm{e}^{-\mathrm{i}h_qd}$$
$$=C_m(\zeta)\mathrm{e}^{\mathrm{i}hd}, \quad (28)$$

$$\sum_{q=1}^{2}E_{mq}(\zeta)\left[B_q^{\rm e}(\zeta)\frac{h_q}{k_q}-\mathrm{i}C_q^{\rm e}(\zeta)\right]\mathrm{e}^{\mathrm{i}h_qd}$$
$$-\sum_{q=1}^{2}E_{mq}(\zeta)\left[B_q^{\rm e}(\zeta)\frac{h_q}{k_q}-\mathrm{i}C_q^{\rm e}(\zeta)\right]\mathrm{e}^{-\mathrm{i}h_qd}$$
$$=D_m(\zeta)\frac{h}{k_0}\mathrm{e}^{\mathrm{i}hd}, \quad (29)$$

$$\sum_{q=1}^{2}E_{mq}(\zeta)A_q^{\rm h}(\zeta)\mathrm{e}^{\mathrm{i}h_qd}$$
$$+\sum_{q=1}^{2}F_{mq}(\zeta)A_q^{\rm h}(\zeta)\mathrm{e}^{-\mathrm{i}h_qd}=D_m(\zeta)\mathrm{e}^{\mathrm{i}hd}, \quad (30)$$

$$\sum_{q=1}^{2}E_{mq}(\zeta)\left[B_q^{\rm h}(\zeta)\frac{h_q}{k_q}-\mathrm{i}C_q^{\rm h}(\zeta)\right]\mathrm{e}^{\mathrm{i}h_qd}$$
$$-\sum_{q=1}^{2}E_{mq}(\zeta)\left[B_q^{\rm h}(\zeta)\frac{h_q}{k_q}-\mathrm{i}C_q^{\rm h}(\zeta)\right]\mathrm{e}^{-\mathrm{i}h_qd}$$
$$=D_m(\zeta)\frac{h}{k_0}\mathrm{e}^{\mathrm{i}hd}. \quad (31)$$

For an incident plane wave, the surface integrals in Eqs. (22)–(25) can be analytically evaluated as has been treated in Refs. [8–10]. As an example, for $\boldsymbol{E}^i=\hat{y}E_0\mathrm{e}^{\mathrm{i}k_0(-x\sin\beta+z\cos\beta)}$ the integral in Eq. (24) becomes

$$\int_0^{\infty}r\mathrm{d}r\int_0^{2\pi}\boldsymbol{E}^i|_{z=0}\times\boldsymbol{n}_{(-m)\lambda}^{(1)}\cdot\hat{z}\mathrm{d}\phi$$
$$=2\pi\mathrm{i}^m\delta(\zeta-\beta)/k_0. \quad (32)$$

For a large number of shaped beams, such as a fundamental Gaussian beam and Hermite–Gaussian beam, these surface integrals can be evaluated numerically, *e.g.*, by the well-known Simpson's 1/3 rule in our programming with MATLAB.

The expansion coefficients can be determined from the system consisting of Eqs. (22)–(25) and (28)–(31). In the following calculations, we truncate the infinite series expansions and integrals by setting $m=-M,-M+1,\ldots,M$ and $r=0$ to $N\lambda_0$ (λ_0 being the wavelength of the incident shaped beam), where M and N are determined by repeating the calculation for successively larger values of M and N (usually larger than 25 and 20 respectively) to ensure a better accuracy of convergence (three or more figures of accuracy, *i.e.*, the first three or more figures of the numerical result remain unchanged with the increase of M and N).

3. Numerical results and discussion

In this section, we will compute the normalized FIDs within different regions where $z<0$, $0<z<d$, and $z>d$, which are respectively defined as

$$\left|(\boldsymbol{E}^i+\boldsymbol{E}^{\rm r})/E_0\right|^2$$
$$=(\left|E_r^i+E_r^{\rm r}\right|^2+\left|E_\phi^i+E_\phi^{\rm r}\right|^2+\left|E_z^i+E_z^{\rm r}\right|^2)/|E_0|^2, \quad (33)$$

$$\left|(\boldsymbol{E}_1^{\rm w}+\boldsymbol{E}_2^{\rm w})/E_0\right|^2$$
$$=(|E_{1r}^{\rm w}+E_{2r}^{\rm w}|^2+\left|E_{1\phi}^{\rm w}+E_{2\phi}^{\rm w}\right|^2+\left|E_{1z}^{\rm w}+E_{2z}^{\rm w}\right|^2)/|E_0|^2, \quad (34)$$

$$\left|\boldsymbol{E}^{\rm t}/E_0\right|^2=(\left|E_r^{\rm t}\right|^2+\left|E_\phi^{\rm t}\right|^2+\left|E_z^{\rm t}\right|^2)/|E_0|^2, \quad (35)$$

where E_0 is the amplitude of electric field of the incident shaped beam in its center O'.

We first consider the propagation properties of a fundamental $\mathrm{TEM}_{00}^{(x')}$ mode Gaussian beam, with its third-order corrected expressions in $O'x'y'z'$ expressed as[15–17]

$$E_x'=E_0[1+s^2(\mathrm{i}Q^3\rho^4-Q^2\rho^2-2Q^2\xi^2)]\psi_0\exp(\mathrm{i}k_0z'), \quad (36)$$
$$E_y'=-E_0s^2 2Q^2\xi\eta\psi_0\exp(\mathrm{i}k_0z'), \quad (37)$$
$$E_z'=E_0[s2Q\xi+s^3(2\mathrm{i}Q^4\rho^4\xi-6Q^3\rho^2\xi)]\psi_0\exp(\mathrm{i}k_0z'), \quad (38)$$
$$H_x'=-\frac{E_0}{\eta_0}s^2 2Q^2\xi\eta\psi_0\exp(\mathrm{i}k_0z'), \quad (39)$$
$$H_y'=\frac{E_0}{\eta_0}[1+s^2(\mathrm{i}Q^3\rho^4-Q^2\rho^2-2Q^2\eta^2)]\psi_0\exp(\mathrm{i}k_0z'), \quad (40)$$
$$H_z'=\frac{E_0}{\eta_0}[s2Q\eta+s^3(2\mathrm{i}Q^4\rho^4\eta-6Q^3\rho^2\eta)]\psi_0\exp(\mathrm{i}k_0z'), \quad (41)$$

where $\xi=x'/w_0$, $\eta=y'/w_0$, $\rho^2=\xi^2+\eta^2$, $Q=1/(\mathrm{i}-2k_0z's^2)$, $s=1/(k_0w_0)$, and $\psi_0(\xi,\eta,\zeta)=\mathrm{i}Q\exp(-\mathrm{i}\rho^2Q)$ are the non-dimensional parameters, and w_0 is the Gaussian beam waist radius.

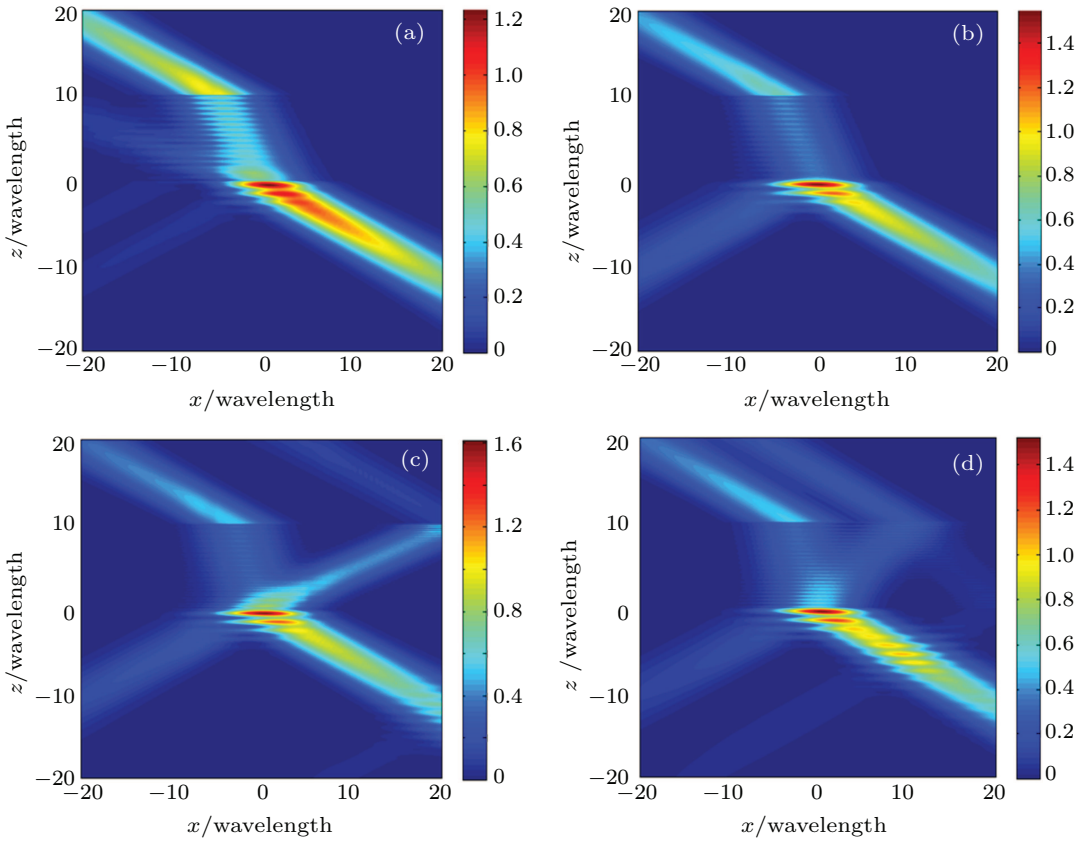


Fig. 2. Normalized FIDs in xOz plane for UAC slab illuminated by $\mathrm{TEM}_{00}^{(x')}$ mode Gaussian beam when $w_0 = 3\lambda$, $z_0 = 0$, $\beta = \pi/3$, $d = 10\lambda_0$, $\varepsilon_z = 2\varepsilon_0$, $\varepsilon_t = \varepsilon_0$, $\mu = \mu_0$, (a) $\kappa = 0.4$, (b) $\kappa = 0.8$, (c) $\kappa = 1.6$, (d) $\kappa = 2$.

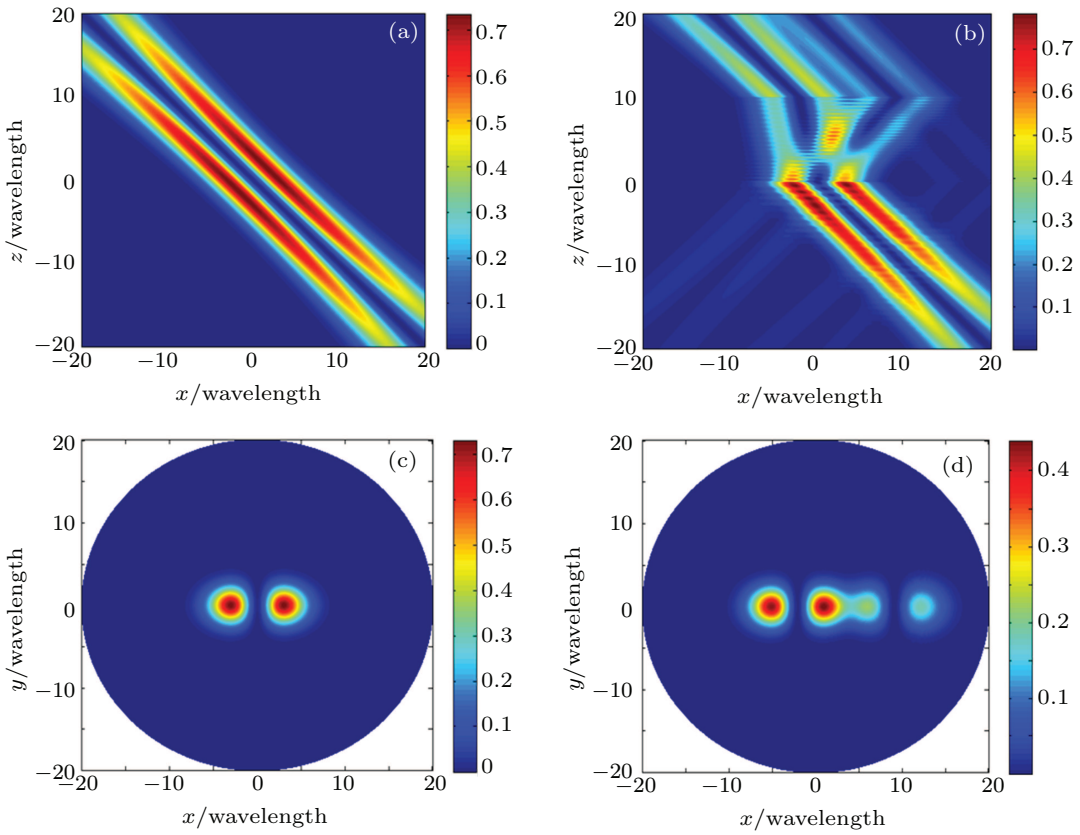


Fig. 3. (a) Normalized FID in xOz plane for $\mathrm{TEM}_{10}^{(x')}$ mode Hermite–Gaussian beam when $w_0 = 3\lambda$, $z_0 = 0$, $\beta = \pi/4$; (b) normalized FID in xOz plane for the same model as that in Fig. 2(d) when $d = 10\lambda_0$, $\varepsilon_z = 2\varepsilon_0$, $\varepsilon_t = \varepsilon_0$, $\mu = \mu_0$, $\kappa = 2$, illuminated by the above Hermite–Gaussian beam; normalized FIDs for the above Hermite–Gaussian beam $\left|\boldsymbol{E}^i/E_0\right|^2$ in (c) $z = 0$ plane, and for the transmitted beam $\left|\boldsymbol{E}^{\mathrm{t}}/E_0\right|^2$ in (d) $z = d$ plane.

Figure 2 shows the normalized FIDs for a $\mathrm{TEM}_{00}^{(x')}$ mode Gaussian beam incident on a UAC slab. For the weak chirality cases where in Eq. (8) $A_1 > 0$ and $A_2 > 0$, in Fig. 2(a) two eigen waves characterized by the wave numbers k_q $(q = 1, 2)$ in Eq. (7) are obviously observed within the UAC slab, and in Fig. 2(b) only one eigen wave corresponding to k_1 appears because the others corresponding to k_2 are attenuated much more quickly. For the strong chirality case where $A_1 > 0$ and $A_2 < 0$, figures 2(c) and 2(d) show that the negative refraction phenomenon happens for one eigen wave corresponding to k_2, and in addition, for a smaller chirality parameter κ the negative refraction is stronger.

Expressions of EM components for a higher-order Hermite–Gaussian beam can be derived by performing transverse derivatives of $\mathrm{TEM}_{00}^{(x')}$ as[17]

$$\mathrm{TEM}_{mn}^{(x')} = \frac{\partial^m \partial^n \mathrm{TEM}_{00}^{(x')}}{\partial \xi^m \partial \eta^n}.$$

Figure 3 shows the normalized FIDs for the same model as that in Fig. 2(d), but the latter in subjected to the illumination by a $\mathrm{TEM}_{10}^{(x')}$ mode Hermite–Gaussian beam. To demonstrate clearly its propagation properties through the UAC slab, both the FID profiles in the xOz plane and in the xOy plane are displayed.

In Fig. 3, the negative refraction phenomena are evidently observed through the interfaces $z = 0$ and $z = d$. We can also see that the Hermite–Gaussian beam splits into four distinct beams after transmitting through the UAC slab.

4. Conclusions

With the EM field expanding in terms of appropriate CVWFs, the boundary conditions and MoM procedure, an approach to computing the reflection and transmission of an incident shaped beam by an infinite UAC slab is presented. By taking a fundamental Gaussian beam and Hermite–Gaussian beam for examples, the normalized FIDs are calculated. Numerical results show that for the different chirality cases, the shaped beam propagation characteristics are markedly different, which can be used to realize a negative refraction or reshape an shaped beam. As a result, the present study provides a general theoretical procedure applicable for arbitrary shaped beams provided that their explicit descriptions are known.

References

[1] Pendry J B 2004 *Science* **306** 1353

[2] Fedotov V A, Mladyonov P L, Prosvirnin S L, Rogacheva A V, Chen Y and Zheludev N I 2006 *Phys. Rev. Lett.* **97** 167401

[3] Tang Y Q and Cohen A E 2010 *Phys. Rev. Lett.* **104** 163901

[4] Klimov V V, Zabkov I V, Pavlov A A, Shiu R C, Chan H C and Guo G Y 2016 *Opt. Express* **24** 6172

[5] Yu S, Park H S, Piao X J, Min B and Park N 2016 *Optica* **3** 1025

[6] Bayatpur F, Amirkhizi A V and Nemat-Nasser S 2012 *IEEE Trans. Microwave Theory Tech.* **60** 1126

[7] Uckun S 1998 *Microwave Opt. Tech. Lett.* **18** 171

[8] Cheng Q and Cui T J 2006 *Phys. Rev. B* **73** 113104

[9] Cheng Q and Cui T J 2006 *J. Opt. Soc. Am. A* **23** 3203

[10] Dong J F and Li J 2012 *Progress In Electromagnetics Research* **127** 389

[11] Zhang H Y, Huang Z X and Shi Y 2013 *Opt. Express* **21** 15645

[12] Wang M J, Zhang H Y, Liu G S, Li Y L and Dong Q F 2014 *Opt. Express* **22** 3705

[13] Stratton J A 1941 *Electromagnetic Theory* (New York: McGraw-Hill Companies) Chap. VII

[14] Tai C T 1971 *Dyadic Green's Functions in Electromagnetic Theory* (New York: International Textbook Company) Chap. 1

[15] Davis L W 1979 *Phys. Rev. A* **19** 1177

[16] Barton J P and Alexander D R 1989 *J. Appl. Phys.* **66** 2800

[17] Barton J P 1997 *Appl. Opt.* **36** 1303